

# Observation of the Kohn anomaly near the K point of bilayer graphene

D. L. Mafra<sup>1</sup>, L. M. Malard<sup>1</sup>, S. K. Doorn<sup>2</sup>, H. Htoon<sup>2,3</sup>, J. Nilsson<sup>4</sup>, A. H. Castro Neto<sup>5</sup>, and M. A. Pimenta<sup>1</sup>

<sup>1</sup>*Departamento de Física, Universidade Federal de Minas Gerais, 30123-970, Belo Horizonte, Brazil.*

<sup>2</sup>*Chemistry Division, Los Alamos National Laboratory, Los Alamos, New Mexico 87545, USA.*

<sup>3</sup>*Center for Integrated Nanotechnologies, Los Alamos National Laboratory, Los Alamos, New Mexico 87545, USA.*

<sup>4</sup>*Instituut-Lorentz, Universiteit Leiden, P.O. Box 9506, 2300 RA Leiden, The Netherlands.*

<sup>5</sup>*Department of Physics, Boston University, 590 Commonwealth Avenue, Boston, Massachusetts 02215, USA.*

(Dated: October 13, 2018)

The dispersion of electrons and phonons near the K point of bilayer graphene was investigated in a resonant Raman study using different laser excitation energies in the near infrared and visible range. The electronic structure was analyzed within the tight-binding approximation, and the Slonczewski-Weiss-McClure (SWM) parameters were obtained from the analysis of the dispersive behavior of the Raman features. A softening of the phonon branches was observed near the K point, and results evidence the Kohn anomaly and the importance of considering electron-phonon and electron-electron interactions to correctly describe the phonon dispersion in graphene systems.

PACS numbers: 63.20.D-, 63.20.kd, 78.30.Na, 81.05.Uw

Graphene systems exhibit a strong electron-phonon coupling at special points in the Brillouin zone, that softens the phonon energy and gives rise to kinks in the phonon dispersion (infinities in  $\partial\omega/\partial\mathbf{q}$ ), which are called Kohn anomaly [1, 2]. This effect has been demonstrated experimentally at the  $\Gamma$  point of monolayer and bilayer graphene using gated Raman scattering experiments [3, 4, 5, 6, 7, 8]. However, the electron-phonon coupling is expected to be stronger at the K point [1], but Raman experiments in graphene systems performed with visible light cannot probe phonons near the K point [5]. Moreover, in the case of AB-stacked bilayer graphene, due to its special electronic and phonon structure [9], Raman experiments involve phonons closer to the K point when compared to monolayer graphene [10]. This work presents a resonance Raman investigation of AB-stacked bilayer graphene using many laser lines in the near-infrared (near-IR) and visible range. The Kohn anomaly for both symmetric (S) and anti-symmetric (AS) phonons was evidenced, and results show the importance of considering higher renormalization terms such as electron-electron interactions to correctly describe the phonon dispersion near the K point [11]. These effects are especially relevant for understanding the dispersion of electrons and phonons [12, 13, 14] and transport properties in this novel material [9].

In a previous resonance Raman study of bilayer graphene performed in the visible range [15], the electronic structure of bilayer graphene was probed by analyzing the dispersion of  $G'$  Raman band (also called 2D band) as a function of the laser energy, and described within a tight-binding approximation [16, 17, 18] by determining the nearest-neighbors hopping parameters  $\gamma_0$ ,  $\gamma_1$ ,  $\gamma_3$  and  $\gamma_4$ . It was shown in this work that a linear iTO phonon dispersion provided a good fit of the experimental data obtained with visible photons [15].

In the present work, we have extended the range of laser energies, measuring the  $G'$  Raman band with many laser lines in the range 1.33 to 2.81 eV. The measurements

in the near-IR range (1.33 to 1.69 eV) are especially relevant since we can probe phonons that are much closer to the K point. The analysis of the low energy data allowed us to observe a non-linear softening of the phonon branch near the K point, and the significant splitting of the symmetric (S) and anti-symmetric (AS) phonon branches. In particular, we show that the phonon softening is stronger for the S branch. Concerning the electronic structure, we have also considered the in-plane second-neighbor hopping parameter, which is expected to be of the same order as the out-of-plane nearest-neighbor parameters, to describe the  $G'$  Raman band dispersion.

The graphene samples used in this experiment were obtained by a micro-mechanical exfoliation of graphite (Nacional de Grafite, Brazil) on the surface of a Si sample with a 300 nm  $\text{SiO}_2$  coverage. The laser power was kept at 1 mW in order to avoid sample heating. We used He-Cd, Ar-Kr and dye lasers for the laser lines in the visible range (1.91–2.81 eV) and a Ti:Sapphire laser for the excitation in the near-IR range (1.33–1.69 eV).

Figure 1 shows the  $G'$  band of bilayer graphene recorded with 19 different laser lines between 1.33 and 2.81 eV (932 to 440 nm). We can see that both the position and the shape of the  $G'$  band are strongly dependent on the energy of the exciting laser. The  $G'$  band in graphene systems comes from an intervalley double resonance (DR) Raman process [19, 20] that involves one initial electronic state with wavevector  $k$  near the K point, one intermediate electronic state with wavevector  $k'$  near the  $K'$  point, and two in-plane transverse optical (iTO) phonons with wavevectors  $q = k + k'$  [10]. Since photons with different energies excite electrons and phonons with different wavevectors  $k$  and  $q$ , respectively, the dispersion of electrons and phonons near the K point can be measured in when the energy of the incident photons can be tuned [10].

In the case of AB-stacked bilayer graphene, the electronic branches split into two valence bands ( $\pi_1$  and  $\pi_2$ ) and two conduction bands ( $\pi_1^*$  and  $\pi_2^*$ ) [9]. The iTO

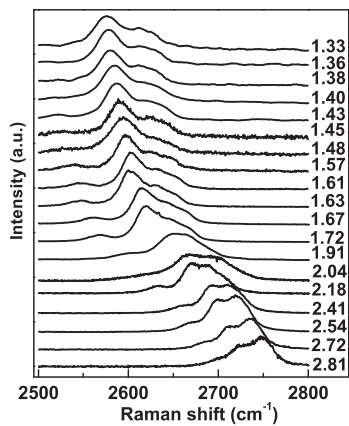


FIG. 1: The Raman  $G'$  band of bilayer graphene recorded with 19 different laser lines between 1.33 and 2.81 eV (932 to 440 nm).

phonon branch also splits into two branches, related to the symmetric (S) and anti-symmetric (AS) phonons. It has been shown that the DR scattering process occurs preferentially in the high symmetric  $\Gamma$ KM direction [21, 22], involving electrons in the  $K\Gamma$  direction and phonons in the KM direction.

Group theory analysis for bilayer graphene [23] predicts four distinct DR processes ( $P_{11}$ ,  $P_{22}$ ,  $P_{12}$  and  $P_{21}$ ) along the  $\Gamma$ KM direction, which are illustrated in Figs. 2(a) and (b). Since the lower and upper conduction bands ( $\pi_1^*$  and  $\pi_2^*$ ) belong to different irreducible representations, the S phonons ( $T_1$  symmetry) are associated with the  $P_{11}$  and  $P_{22}$  processes [see Fig. 2(a)] involving electrons with same symmetry ( $\pi_1^* \rightarrow \pi_1^*$  or  $\pi_2^* \rightarrow \pi_2^*$ ) whereas the AS phonons ( $T_2$  symmetry) occur for processes  $P_{12}$  and  $P_{21}$  [Fig. 2(b)] involving electrons with different symmetries ( $\pi_1^* \rightarrow \pi_2^*$  or  $\pi_2^* \rightarrow \pi_1^*$ ) [15].

Each of these processes ( $P_{11}$ ,  $P_{22}$ ,  $P_{12}$  and  $P_{21}$ ) is responsible for one peak in the  $G'$  band of AB-stacked bilayer graphene. Fig. 2(c) shows the Raman spectrum of the  $G'$  band measured with 1.57 eV laser energy and fitted with four peaks. All have the same FWHM of  $24 \text{ cm}^{-1}$ , which is the FWHM of the single band in monolayer graphene [10, 24]. We see in Fig. 2(a) that the  $P_{11}$  process involves the phonon with higher wavevector, while the phonon with smaller wavevector gives rise to the  $P_{22}$  process. Therefore, the  $P_{22}$  process is especially relevant since it involves phonons closer to the K point, even when compared to the phonon in monolayer graphene probed by the same laser line. Since the iTO phonon frequency increases with increasing  $q$ , we conclude that the lowest and highest frequency peaks of the  $G'$  band are associated with the  $P_{11}$  and  $P_{22}$  processes, respectively. The two intermediate Raman peaks are due to the  $P_{12}$  and  $P_{21}$  processes, as shown in Fig. 2(c).

All  $G'$  bands shown in Fig. 1 were fitted by four Lorentzian curves, and laser energy dependence of the Lorentzian peak positions are plotted in Fig. 3(a-d). In order to analyze the experimental dispersion of the  $G'$

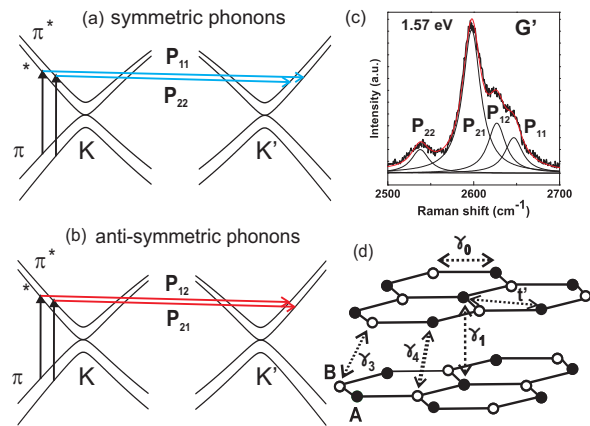


FIG. 2: (Color online) (a)  $P_{11}$  and  $P_{22}$  DR Raman processes involving the symmetric phonon, (b)  $P_{12}$  and  $P_{21}$  DR Raman processes involving the anti-symmetric phonon (c)  $G'$  Raman band of bilayer graphene measured with 1.57 eV laser energy and fitted with four Lorentzian peaks with FWHM of  $24 \text{ cm}^{-1}$ . (d) Bilayer graphene atomic structure showing the hopping processes associated with first-neighbor interactions ( $\gamma_0$ ,  $\gamma_1$ ,  $\gamma_3$  and  $\gamma_4$ ), and second neighbor interaction  $t'$ .

peaks shown in Fig. 3(a-d), we need to consider the dispersion of both electrons and phonons near the K point. The electronic dispersion will be analyzed here using the tight-binding approximation, which was first introduced by Wallace [18], using the Slonczewski-Weiss-McClure (SWM) [16, 17] model for graphite, and the phonon dispersion is obtained from the fit of the experimental data.

In the previous resonance Raman study in bilayer graphene performed in the visible range [15], a linear phonon dispersion was considered to fit the  $G'$  peak positions versus  $E_{laser}$  data. Fig. 3(a) shows that the fitting of the data of the present study considering the linear phonon dispersion and the SWM parameters used in reference [15] fails for the experimental points in the near-IR region and, in particular, for the data associated with the  $P_{22}$  process involving phonons closer to the K point.

In order to fit the low energy experimental data in Fig. 3, we have considered a non-linear relation for the iTO phonon dispersion, given by a second-order polynomial  $w(q) = A + Bq + Cq^2$ . Fig. 3(b) shows the fit considering the same non-linear phonon dispersion for the S and AS phonon branches, and the  $\gamma_0$ ,  $\gamma_1$ ,  $\gamma_3$ ,  $\gamma_4$  parameters. Fig. 3(c) shows the fit using the same SWM parameters as in Fig. 3(b) but considering two distinct non-linear phonon dispersions for the S and AS branches. As we can see in Fig. 3(b) and (c), the fitting in the low energy range is improved considering the non-linear dispersion, but different dispersions for the S and AS branches are needed to obtain a good fit of the experimental data. All fitting parameters are shown in Table I.

In the fittings shown in Figs. 3(a)-(c), we have considered only the first-neighbor parameters  $\gamma_0$ ,  $\gamma_1$ ,  $\gamma_3$ ,  $\gamma_4$ . In principle, we could also introduce higher-order terms and, in particular, the in-plane second-neighbor parameter  $t'$ ,

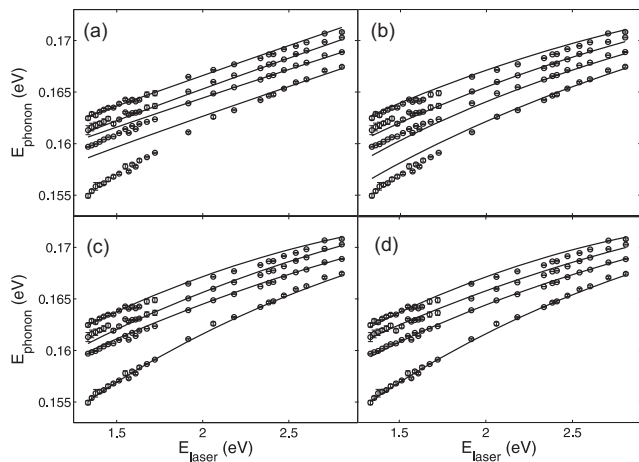


FIG. 3: Laser energy dependence of the peaks of the  $G'$  bands, fitted considering four different approximations. (a) Fitting considering linear phonon dispersion and the SWM parameters  $\gamma_0, \gamma_1, \gamma_3, \gamma_4$  (same approximation as in Ref. [15]). (b) Fitting considering the same non-linear phonon dispersion for the S and AS branches, and the SWM parameters  $\gamma_0, \gamma_1, \gamma_3, \gamma_4$ . (c) Fitting considering different non-linear phonon dispersions for the S and AS phonon branches, and the same SWM as in (b). (d) Fitting using the same phonon dispersions as in (c), the first-neighbor SWM parameters  $\gamma_0, \gamma_1, \gamma_3, \gamma_4$ , second-neighbor in-plane  $t'$  parameter, and the  $\Delta$  parameter, which represents the difference in energy of the sublattices A and B. All fitting parameters used in approximations (a), (b), (c) and (d) are shown in Table I.

which is expected to be of the same order of magnitude as the out-of-plane first-neighbor parameters. Figure 3(d) shows the fit of the experimental data considering also  $t'$  and  $\Delta$ , which represents the difference in energy of the sublattices A and B. As we observe in Figure 3(d), the resultant fit is slightly improved, mainly due to the use of larger number of fitting parameters.

It is important to emphasize that slightly different values of the  $\gamma$  parameters are found when we include  $t'$  and  $\Delta$ . A good fit can always be obtained for  $\gamma_0$  values ranging between 2.9 and 3.1 eV. Concerning the  $\gamma_1$  parameter, reasonable fits could only be obtained for  $\gamma_1 < 0.35$  eV, in disagreement with values of  $\gamma_1$  up to 0.4 eV proposed in the literature [25, 26, 27]. Considering the  $\gamma_3$  parameter, the best fit is obtained when  $\gamma_3 \approx 0.1$  eV, and a reasonable fit cannot be obtained for values of  $\gamma_3 > 0.15$  eV. Once again, this value is smaller than others found in the graphite literature ( $\gamma_3 \approx 0.30$  eV [28, 29, 30]). Recent infrared studies in exfoliated bilayer graphene consider  $\gamma_3 \approx 0.30$  eV [31, 32], but this value is not extracted directly from the experiments [25, 27]. Notice that  $\gamma_3$  is related to the trigonal warping effect (TWE) at very low energies and gives rise to electron-hole pockets [33] in the energy scale of  $\sim 2$  meV, which is not accessible in Raman experiments. However as the energy increases, there is also a TWE due to the symmetry of the lattice, which is probed by our experiment. These two effects

can explain the different  $\gamma_3$  values found with distinct experimental techniques.

If we consider only nearest neighbor parameters to describe the electronic structure, the best fit is obtained for  $\gamma_4 \approx 0.15$  eV, which is in close agreement with our previous experiment [15] and with Refs. [25, 26]. However, smaller values of  $\gamma_4$  provide a good fit when the second-neighbor  $t'$  parameter is included. In fact, both  $\gamma_4$  and  $t'$  parameters are associated with the asymmetry between electrons and holes in bilayer graphene. Finally, reasonable fits can be obtained for different small positive and negative values of  $\Delta$  ( $|\Delta| < 0.01$  eV).

The analysis of the experimental data also gives us the phonon dispersion for the symmetric (S) and anti-symmetric (AS) iTO phonon branches near the K point. As shown in Figs.3(c) and (d), two distinct phonon branches, associated with symmetric and anti-symmetric iTO phonons, are necessary to fit the experimental data. The values of the polynomial parameters  $A, B$  and  $C$  for the S and AS branches are shown in Table I. We observe that the quadratic coefficients  $C$  assume negative values, showing that the slope of the phonon dispersion increases with decreasing  $q$  values. This is direct evidence of the Kohn anomaly for the iTO phonon branches, which are expected to exhibit a kink at the K point.

The experimental data shown in Fig. 3 can be directly plotted in a phonon energy dispersion relation ( $\omega_{ph}$  versus  $q$ ) by eliminating the laser energy ( $E_{laser}$ ) in the double resonance conditions [15]. Fig.4 shows the phonon dispersion of the S (full circles) and AS (open circles) branches obtained from the resonance Raman results, considering the same TB parameters as in Fig.3(c). Fig. 4 also shows the theoretical phonon dispersion near the Dirac point of the iTO phonon branch of monolayer graphene calculated using the tight-binding approximation by Popov *et al.* [34] (solid curve) and using DFT by Lazzeri *et al.* [11] (dashed curve) within the  $GW$  approximation, where electron-electron interaction is taken into account. Notice that the phonon dispersion calculated by tight-binding fails to describe the data for lower phonon energies, which are in good agreement with the calculations within the  $GW$  approximation. This result shows the importance of considering electron-phonon and electron-electron interactions in order to correctly describe the phonon dispersion near the K point of graphene systems.

Another interesting observation is the fact that the phonon softening is stronger for the S phonon branch as shown in Fig.4. This result is in agreement with the calculation performed by Ando *et al.* [35], which predicts a stronger phonon renormalization for the zone-center symmetric phonon, due to distinct selection rules for interaction of S and AS phonons with intra-valley and inter-valley electron-hole pairs. The same type of selection rule is expected to occur for phonons near the K point.

In summary, the dispersion of electrons and phonons of bilayer graphene was investigated by performing a res-

TABLE I: Values of the SWM parameters (in units of eV) and the iTO phonon dispersion parameters ( $w(q) = A + Bq + Cq^2$ ) obtained from the four different fits of the experimental data shown in Fig.3 (a), (b), (c) and (d).

	$\gamma_0$	$\gamma_1$	$\gamma_3$	$\gamma_4$	$\Delta$	$t'$	symmetric			anti-symmetric		
							A(meV)	B(meVÅ)	C(meVÅ <sup>2</sup> )	A(meV)	B(meVÅ)	C(meVÅ <sup>2</sup> )
(a)	2.9	0.3	0.1	0.12	-	-	153.7	38.5	-	154.0	38.8	-
(b)	3.0	0.35	0.1	0.15	-	-	149.3	69.5	-46.6	149.3	69.5	-46.6
(c)	3.0	0.35	0.1	0.15	-	-	146.3	86.9	-70.3	150.5	66.3	-44.8
(d)	3.0	0.35	0.1	0.10	0.01	0.15	146.3	86.9	-70.3	150.5	66.3	-44.8

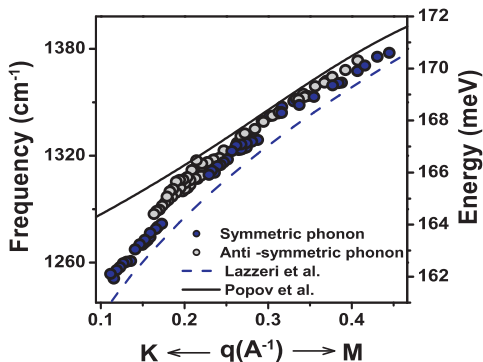


FIG. 4: (Color online) Experimental iTO phonon dispersion of bilayer graphene near the K point of the S (full circles) and AS (open circles) branches. The solid and dashed curves correspond, respectively, to the theoretical iTO phonon dispersion of monolayer graphene calculated using tight-binding by Popov *et al.* [34] and using DFT by Lazzeri *et al.* [11] within the *GW* approximation.

onance Raman study of the the G' Raman band, using

laser energies from the visible to the near-IR range. The measurements in the near-IR range are especially relevant since we can probe phonons that are much closer to the K point. The electronic structure was analyzed within the tight-binding approximation, considering first and second neighbor interactions. We have obtained accurate experimental data for the phonon dispersion of the iTO branches near the K point, and the phonon branch softening reveals the K point Kohn anomaly in bilayer graphene. We have shown that the phonon renormalization is stronger for the S phonon branch. Our results agree with the phonon dispersion calculation which takes into account electron-electron interaction in graphene systems, which plays an important role to correctly describe the Kohn anomaly near the K point.

This work was supported by Rede Nacional de Pesquisa em Nanotubos de Carbono - MCT, and the Brazilian Agencies CNPq and FAPEMIG. Resonance Raman studies in the near infrared range were conducted at the Center for Integrated Nanotechnologies, jointly operated by Los Alamos and Sandia National Laboratories

- 
- [1] S. Piscanec *et al.*, Phys. Rev. Lett. **93**, 185503 (2004).
  - [2] W. Kohn, Phys. Rev. Lett. **2**, 393 (1959).
  - [3] S. Pisana *et al.*, Nature Mater. **6**, 198 (2007).
  - [4] J. Yan *et al.*, Phys. Rev. Lett. **98**, 166802 (2007).
  - [5] A. Das *et al.*, Nature Nanotech. **3**, 210 (2008).
  - [6] A. Das *et al.*, Phys. Rev. B **79**, 155417 (2009).
  - [7] J. Yan *et al.*, Phys. Rev. Lett. **101**, 136804 (2008).
  - [8] L. M. Malard *et al.*, Phys. Rev. Lett. **101**, 257401 (2008).
  - [9] A. H. Castro Neto *et al.*, Rev. Mod. Phys. **81**, 109 (2009).
  - [10] L. M. Malard *et al.*, Phys. Rep. **473**, 51 (2009).
  - [11] M. Lazzeri *et al.*, Phys. Rev. B. **78**, 081406(R) (2008).
  - [12] A. Bostwick *et al.*, Nat. Phys. **3**, 36 (2007).
  - [13] A. Grüneis *et al.*, Phys. Rev. Lett. **100**,
  - [14] A. Grüneis *et al.*, arXiv:0904.3205 (2009).
  - [15] L. M. Malard *et al.*, Phys. Rev. B **76**, 201401 (2007).
  - [16] J. W. McClure, Phys. Rev. **108**, 612 (1957).
  - [17] J. C. Slonczewski and P. R. Weiss, Phys. Rev. **109**, 272 (1958).
  - [18] P. R. Wallace, Phys. Rev. **71**, 622 (1947).
  - [19] C. Thomsen and S. Reich, Phys. Rev. Lett. **85**, 5214 (2000).
  - [20] R. Saito *et al.*, Phys. Rev. Lett. **88**, 027401 (2002).
  - [21] J. Maultzsch *et al.*, Phys. Rev. B **70**, 155403 (2004).
  - [22] D. L. Mafra *et al.*, Phys. Rev. B **76**, 233407 (2007).
  - [23] L. M. Malard *et al.*, Phys. Rev. B **79**, 125426 (2009).
  - [24] A. C. Ferrari *et al.*, Phys. Rev. Lett. **97**, 187401 (2006).
  - [25] L. M. Zhang *et al.*, Phys. Rev. B **78**, 235408 (2008).
  - [26] Z. Q. Li *et al.*, Phys. Rev. Lett. **102**, 037403 (2009).
  - [27] A. B. Kuzmenko *et al.*, Phys. Rev. B **79**, 115441 (2009).
  - [28] M.S. Dresselhaus, G. Dresselhaus, K. Sugihara, I. L. Spain and H. A. Goldberg, Carbon Fibers and Filaments, Chapter 7, Springer Verlag (Berlin Heidelberg) 1988.
  - [29] A. Grüneis *et al.*, Phys. Rev. B **78**, 205425 (2008).
  - [30] J. M. Schneider *et al.*, Phys. Rev. Lett. **102**, 166403 (2009).
  - [31] B. Partoens and F. M. Peeters, Phys. Rev. B **74**, 075404 (2006).
  - [32] H. Min *et al.*, Phys. Rev. B **75**, 155115 (2007).
  - [33] E. McCann and V. I. Fal'ko, Phys. Rev. Lett. **96**, 086805 (2006).
  - [34] V. N. Popov and P. Lambin, Phys. Rev. B **73**, 085407 (2006).
  - [35] T. Ando, J. Phys. Soc. Jpn. **76**, 104711 (2007).